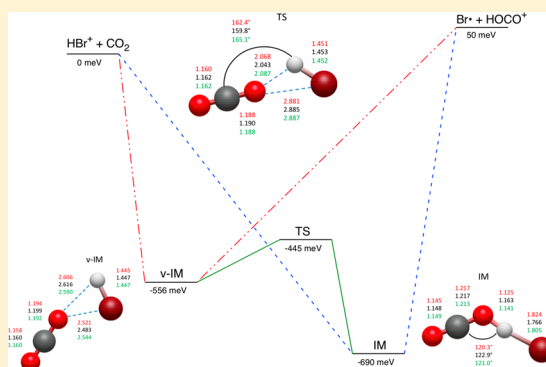


Theoretical Study of the Potential Energy Profile of the $\text{HBr}^+ + \text{CO}_2 \rightarrow \text{HOCO}^+ + \text{Br}\cdot$ Reaction

Alyson Shoji,[†] David Schanzenbach,[‡] Ron Merrill,[‡] Jiaxu Zhang,[§] Li Yang,[§] and Rui Sun^{*,†,§}[†]Department of Chemistry, The University of Hawai'i at Manoa, Honolulu, Hawaii 96822, United States[‡]Information Technology Services, The University of Hawai'i, Honolulu, Hawaii 96822, United States[§]MIT Key Laboratory of Critical Materials Technology for New Energy Conversion and Storage, School of Chemistry and Chemical Engineering, Harbin Institute of Technology, Harbin 150001, P. R. China

Supporting Information

ABSTRACT: Recent guided ion beam experiments have revealed interesting reaction dynamics of the $\text{HBr}^+ + \text{CO}_2 \rightarrow \text{HOCO}^+ + \text{Br}\cdot$ reaction under different conditions. The hypothesis is that the predominant reaction mechanism depends on the collision energy between two reactants, the angular momentum of HBr^+ , and the spin-orbit coupling state of the system. The potential energy profile of the $\text{HBr}^+ + \text{CO}_2 \rightarrow \text{HOCO}^+ + \text{Br}\cdot$ reaction is studied in this research to lay the groundwork for an ab initio molecular dynamics simulation. First, a benchmark potential energy profile of this reaction is identified using coupled-cluster theory extrapolated to the complete basis set limit. A transition state connecting the previously reported intermediates is found, making the potential energy surface of the $\text{HBr}^+ + \text{CO}_2 \rightarrow \text{HOCO}^+ + \text{Br}\cdot$ reaction double-welled. Second, various single reference ab initio methods are compared with the benchmark potential energy profile to search for the most suitable ab initio method for the dynamics simulation. Two combinations of double- ζ basis sets (with effective core potentials) with MP2 and density functional theory have been identified to accurately represent the potential energy profile of this reaction.



I. INTRODUCTION

Reaction dynamics answers questions of why chemical reactions occur, how to predict their behavior, and how to control them.¹ Starting with simple, elementary reactions, the knowledge of the reaction process at a microscopic level allows for the further application of fundamental theories to other more complex and important reactions. Aside from external conditions such as temperature and pressure, the reaction dynamics depends heavily on the reaction free energy surface (FES), which is composed of its intrinsic potential energy surface (PES) and the entropy of the system. For an elementary reaction, the contribution from the entropy of the system to the FES has been well studied and implemented in various rate constant theories, for example, transition state theory (TST)² and Rice–Ramsperger–Kassel–Marcus (RRKM) theory.³ Furthermore, the PES varies from system to system, and numerous experimental and computational studies have been devoted to understanding its impact on the rate, pathways, and yields of a reaction.

The dynamics of ion–molecule gas-phase reactions is of great importance in a variety of fields, including the study of interstellar clouds,⁴ plasma chemistry,⁵ and analytical mass spectrometry.⁶ Understanding the influence of different excitations of ion–molecule reactions provides valuable insight for scientists to design and manipulate the reaction process. In

Paetow et al.'s recent guided ion beam experiments,^{7,8} the reaction dynamics of $\text{HBr}^+ + \text{CO}_2 \rightarrow \text{HOCO}^+ + \text{Br}\cdot$ was investigated under different conditions and showed non-intuitive phenomena. Paetow et al. measured the dependency of the reaction probability on (1) the collision energy between HBr^+ and CO_2 , (2) the rotational energy of HBr^+ , (3) the angular momentum of HBr^+ , and (4) the spin–orbit states of HBr^+ . The results of this guided ion beam experiment revealed that the reaction probability increased with the increase in collision energy between HBr^+ and CO_2 . It was also found that the rotational energy of HBr^+ played an increasingly more important role in the reaction probability as the collision energy increased. For example, with relatively high collision energies ($E_{\text{col}} > 0.85$ eV), the reaction probability decreased by $\sim 55\%$ as the rotational energy increased from 1.4 to 66.3 meV; however, with lower collision energies ($E_{\text{col}} < 0.35$ eV), the reaction probability decreased by only $\sim 35\%$. In another experiment, Paetow et al. further studied this reaction by exciting HBr^+ from its ground spin–orbit coupling state ($^2\Pi_{3/2}$) to the excited spin–orbit coupling state ($^2\Pi_{1/2}$), which changed the reaction from endothermic to exothermic. The

Received: August 11, 2019

Revised: October 17, 2019

Published: October 21, 2019

correlation between the reaction probability and the rotation of HBr^+ is completely different from the ground state of HBr^+ : The reaction probability is independent of the rotation of HBr^+ with high (>1 eV) and low (<0.23 eV) collision energy but has a negative correlation with the rotation of HBr^+ when the collision energy is moderate (between 0.25 and 0.85 eV).⁸ Paetow et al.'s studies shed light on the complicated dynamics of the $\text{HBr}^+ + \text{CO}_2 \rightarrow \text{HOCO}^+ + \text{Br}^-$ reaction, especially on how the reaction proceeded under different excitations. Nevertheless, because of the limit in the resolution of the guided ion beam experiments, a lack of understanding of the atomistic mechanism of this reaction remains. Therefore, it is of interest to study this reaction with ab initio molecular dynamics (AIMD)^{9,10} simulations, in which the time evolution of the positions of the atoms can be tracked in real time.^{11–13}

The accuracy of AIMD simulations relies on three factors: First, a representative sampling must reproduce the experimental conditions. Second, the number of trajectories must be sufficiently large for a reliable statistical analysis of the results. Last, the ab initio calculations should be capable of precisely modeling the PES of the reaction. The first two factors demand a large number of trajectories (usually at least a couple of thousand) that correspond to a thermodynamics ensemble to be sampled. Each of the trajectories is propagated with forces (i.e., energy gradients) computed from ab initio calculations and is therefore composed of up to tens of thousands of ab initio calculations. Because of the amount of ab initio calculations required in AIMD, there must be a balance between the cost and the accuracy of the computation. Therefore, a single reference method, such as density functional theory (DFT)¹⁴ or second-order Møller–Plesset perturbation theory (MP2)¹⁵ with double- ζ basis sets, is often selected for AIMD simulations.^{9,10}

As of now, the experimental heat of formation is only available for the reactants and products of the $\text{HBr}^+ + \text{CO}_2 \rightarrow \text{HOCO}^+ + \text{Br}^-$ reaction. The first theoretical study of this reaction was conducted by Sun et al. in 2015,¹⁶ where the potential energies of the critical points on the PES were calculated using CCSD(T)¹⁷ with double- ζ and triple- ζ (correlation consistent) basis sets¹⁸ and then extrapolated to the complete basis set (CBS) limit.^{19,20} To search for a proper method for the AIMD study, a series of DFT and MP2 calculations with various basis sets and effective core potentials (ECPs)^{21–23} were calculated and compared against the benchmark potential energies. MP2/cc-pVTZ/PP was proposed by Sun et al. as a candidate level of theory for the dynamic study.¹⁶ The speed of an energy gradient calculation with MP2/cc-pVTZ/PP of this reaction system was tested and yields ~ 50 s with NWChem (version 6.6)²⁴ on one computer node, which contains two Intel Xeon E5-2680v2 “Ivy Bridge” 10-core, 2.8 GHz processors (20 CPUs total). As previously discussed, up to millions of energy gradient calculations are necessary for one set of AIMD simulations of this system; therefore, the MP2/cc-pVTZ/PP level of theory would require hundreds of thousands of node hours. To compare with the guided ion beam experiments by Paetow et al.,^{7,8} several sets of AIMD simulations (e.g., with different collision energies) need to be conducted, and, as a result, the MP2/cc-pVTZ/PP level of theory makes the computational cost unaffordable. It is worth noting that several recently developed DFT functionals (especially the commonly used Minnesota functionals)^{25–27} and ECPs (for bromine) were absent from the previous study by Sun et al.¹⁶ Therefore, our goal is to carry out a

comprehensive theoretical study in search of a better cost-effective method to model this reaction in an AIMD study.²⁸ A variety of DFT functionals and MP2 are tested with different basis sets and ECPs. The methods that are tested include: B3LYP*,²⁹ Becke98*,³⁰ M05,²⁷ M06,²⁶ M06-L,²⁵ XM06,²⁶ CM06-L,²⁵ XMVS15,³¹ and unrestricted MP2 (UMP2)*.¹⁵ The methods with asterisks (B3LYP, Becke98, and UMP2) were previously studied by Sun et al.¹⁶ Each of these methods is paired with combinations of basis sets (e.g., aug-cc-pVDZ³²/cc-pVDZ³²) combined with various ECPs (e.g., LANL2DZdp, PP, LANL08, and LANL08d). The various types of triple- ζ basis sets, such as cc-pVTZ/PP,^{32–34} are not further tested with MP2 due to their high computational costs. All of the quantum calculations in this study are carried out with NWChem (version 6.6).²⁴

In addition, a transition state (TS in Figure 1) that connects the two previously reported intermediate complexes (a

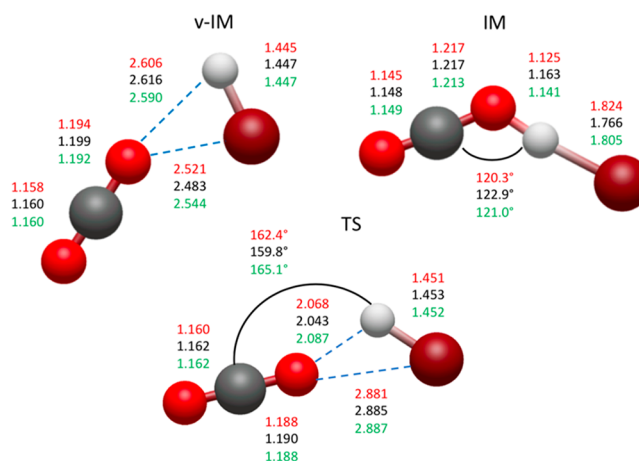


Figure 1. Optimized structures of critical points of the $\text{HBr}^+ + \text{CO}_2 \rightarrow \text{HOCO}^+ + \text{Br}^-$ reaction, with lengths in angstroms and angles in degrees. The numbers are from the geometry optimization of the (top) CCSD(T)/cc-pVDZ/PP, (middle) CCSD(T)/aug-cc-pVDZ/PP, and (bottom) UMP2/cc-pVDZ/LANL08d methods. The vibrational frequencies of these species can be found in Table S1.

hydrogen bond compound (IM) and a van der Waals compound (v-IM) in Figure 1)¹⁶ is reported for the first time in our research. In Sun et al.'s study,¹⁶ it was not clear whether IM and v-IM were able to interconvert into one another by crossing a transition state. As shown in nucleophilic substitution reactions ($\text{S}_{\text{N}}2$), the dynamics of ion–molecule reactions depends heavily on the critical points on the PES.^{13,35,36} Therefore, the ab initio method needs to accurately represent the relative energy difference between the TS and IM and the TS and v-IM. As shown later in this Article, the two single reference methods that reproduce the benchmark energies are UMP2/cc-pVDZ/lanl08d and XMVS15/cc-pVDZ/PP. These two methods will be considered for the future AIMD simulations. Compared with the previous selected MP2/cc-pVTZ/PP level of theory, the computational costs of UMP2/cc-pVDZ/lanl08d and XMVS15/cc-pVDZ/PP are reduced by 90 and 60%, respectively, while also sharing a similar accuracy in reproducing the benchmark potential energy.

This Article is organized as follows: The method for generating the experimental and theoretical benchmark potential energy profile, the criteria for comparing different

single reference calculations, and the procedure of searching for a TS are introduced in the [Methods](#) section. The [Results](#) section includes the benchmark potential energy profile, the performance of various DFTs and MP2 calculations, and the structure of the TS connecting the two intermediates. This Article concludes with a discussion of our results and the future AIMD study.

II. METHODS

II.a. Benchmark Potential Energies. A reference potential energy profile must be in place to test for a more computationally effective ab initio method. The most reliable energy reference is the experimental heats of formation. The experimental heats of formation (0 K, taken from Active Thermochemical Tables³⁷) for the $\text{HBr}^+ + \text{CO}_2 \rightarrow \text{HOCO}^+ + \text{Br}$ reaction are CO_2 , -393.107 ± 0.014 kJ/mol; HBr^+ ($^2\Pi_{1/2}$), 1097.71 ± 0.14 kJ/mol; HOCO^+ , 600.80 ± 0.45 kJ/mol; and Br ($^2P_{3/2}$), 117.92 ± 0.06 kJ/mol,^{7,8,16} yielding the experimental heat of reaction of 146 ± 5 meV. The aforementioned reaction energy needs to be further processed before being compared with the reaction energy from quantum calculations (i.e., CCSD(T), DFT, and MP2, all of which are spin-free methods) due to the zero-point energies (ZPEs) of each polyatomic species and spin-orbit coupling effects of HBr^+ and Br . The anharmonic ZPEs of HBr^+ and CO_2 are 153 and 314 meV, respectively, which are calculated using second-order perturbation theory³⁸ with experimental vibrational constants.^{38,39} The vibrational frequencies for the product molecule HOCO^+ have been measured in various studies: OH stretch, 3636 cm^{-1} ;⁴⁰ CO stretch, 1853 cm^{-1} ;⁴¹ HOC bend, 1210 cm^{-1} ; OC stretch, 1050 cm^{-1} ; OCO bend, 615 cm^{-1} ;⁴² and torsion, 508 cm^{-1} .⁴³ With the assumption of harmonic oscillation, it yields a ZPE for the HOCO^+ molecule of 550 meV. It is also important to acknowledge that the experimental heats of formation for HBr^+ ($^2\Pi_{1/2}$) and Br ($^2P_{3/2}$) are measured at their ground spin state, whereas the energies calculated from ab initio methods in our research correspond to a spin-free state. Because the other multiplets of HBr^+ ($^2\Pi_{1/2}$) and Br ($^2P_{3/2}$) are well-separated in energy,¹⁶ the splitting of the $^2\Pi$ multiplet of HBr^+ and of the 2P multiplet of Br is only due to the spin-orbit interaction of the states belonging to the same multiplets. In the Π state of a diatomic with one unpaired electron, as HBr^+ , there are two states where the spin and orbital angular momentum add, resulting in $\pm 3/2$, and two states where they subtract, resulting in $\pm 1/2$. Each of the two pairs of states is degenerate, and the average of the energy from the total four spin-orbit coupling states is simply in the middle. This means that the spin-orbit coupling pushes one pair up and the other down by the same amount, which is half of the splitting. Regarding the Br atom, there are a total of six states: Four have the total angular momentum of $3/2$ (projections on the z axis $+3/2, +1/2, -1/2, -3/2$), which are degenerate and of lower energy; two have the total angular momentum of $1/2$ (projections on the z axis $+1/2, -1/2$) and have a higher energy. As a result, the average energy, that is, the energy without spin-orbit coupling, is $1/3$ of the splitting higher than the $^2P_{3/2}$ ground state. As a result, the energy of the ground spin state for HBr^+ (i.e., $^2\Pi_{1/2}$) is 164 meV lower than that of the spin-free state, and the energy of the ground spin state of Br ($^2P_{3/2}$) is 152 meV lower than that of the spin-free states.^{44–46} As a result, the ZPE-free and spin-free experimental reaction energy at 0 K is 50 ± 5 meV, and this

value can be directly compared to the spin-free ab initio calculations.

In the absence of experimental heats of formation (i.e., TS, IM, and v-IM), CCSD(T)/CBS is generally accepted as a quantum-mechanical method that predicts an accurate absolute energy of a substance at its ground electronic state without spin-orbit coupling.^{19,47} By increasing the size of the basis sets in a hierarchal manner, the CBS limit mimics a calculation with an infinite number of basis functions by extrapolating the energies from double- ζ , triple- ζ , and quadruple- ζ basis sets, therefore yielding an accurate representation of the absolute energy of the system. The CBS limit is calculated by using the equation from Peterson et al.¹⁹

$$E(n) = E_{\text{CBS}} + A \exp[-(n-1)] + B \exp[-(n-1)^2] \quad (1)$$

in which n is the value corresponding to the level of basis set used ($n = 2, 3, 4$, corresponding to double- ζ ($X = D$), triple- ζ ($X = T$), and quadruple- ζ ($X = Q$) basis sets for cc-pVXZ and aug-cc-pVXZ, respectively). E_{CBS} represents the estimated CBS limit energy, and A and B are coefficients. Three unknowns (E_{CBS} , A , and B) can be solved from a set of three equations ($n = 2, 3, 4$).

II.b. Root-Mean-Square Deviation Calculation. The root-mean-square deviation (rmsd) is the measure of differences between two sets of values; therefore, it is employed to help determine whether an ab initio method is accurate to reproduce the potential energy profile of the reaction. The reference values chosen to be compared against are the experimental value of $50 (\pm 5)$ meV for the reaction energy and the CCSD(T)/CBS energies for TS, IM, and v-IM (TS = -445 meV, IM = -690 meV, and v-IM = -556 meV; justification provided in the next section). The equation used to calculate the rmsd is shown in eq 2

$$\text{rmsd} = \sqrt{\frac{1}{4}(\delta_{\text{v-IM}}^2 + \delta_{\text{IM}}^2 + \delta_{\text{RXN}}^2 + \delta_{\text{TS}}^2)} \quad (2)$$

$\delta_{\text{v-IM}}$, δ_{IM} , δ_{RXN} , and δ_{TS} represent the differences between the benchmark energy and the candidate method. An rmsd value is included in the next section only if IM, v-IM, and TS were all successfully optimized. A lower rmsd value indicates that a candidate method is able to accurately represent the four points on the PES (reaction energy, IM, v-IM, and TS) of the reaction.

II.c. Transition-State Search. Depending on the orientation of the reactants, the association of $\text{HBr}^+ + \text{CO}_2$ could lead to two intermediates (IM and v-IM; see [Figure 1](#)), which might be connected by a possible transition state. The geometry of the TS should be a combination of the IM and the v-IM; therefore, a linear interpolation method is used to generate 21 candidate configurations that gradually transition from the IM to the v-IM. An energy calculation is carried out at each configuration. Eight configurations that are adjacent to the maximum energy are used as initial configurations in NWChem to search for a transition state, and they all converged to the same optimized structure (TS; see [Figure 1](#)). A vibrational frequency calculation is then performed to further verify that there is one imaginary frequency associated with this structure.

An intrinsic reaction coordinate (IRC)^{48–50} calculation is performed to determine whether the aforementioned transition

state indeed connects the IM and the v-IM. The IRC algorithm was first developed by Fukui,^{48–50} who stated that it is the path going downhill, starting from the transition state following a gradient on the PES, by solving the following differential equation

$$\frac{dq(s)}{ds} = \nu(s) \quad (3)$$

in which $q(s)$ represents the mass-weighted Cartesian coordinates, s is the coordinate along the IRC, and ν is the normalized tangent vector.⁴⁹

III. RESULTS

III.a. Potential Energy Profile from CCSD(T)/CBS.

Because of its enormous memory requirement, the geometry optimization is performed only with double- ζ basis sets (e.g., cc-pVDZ and aug-cc-pVDZ) for the CCSD(T) calculation. The geometries from these calculations are used for single-point calculations with triple (e.g., cc-pVTZ and aug-cc-pVTZ) and quadruple basis sets (e.g., cc-pVQZ and aug-cc-pVQZ). The results of these calculations are extrapolated to the CBS limit and are summarized in Table 1. The CCSD(T)/CBS

Table 1. Summary of CCSD(T) Calculations and the CBS Limit Values (Extrapolated from Double, Triple, and Quadruple Zeta Basis Sets) for the Reaction Energy ($\Delta_r E$), IM, v-IM, and TS of the $\text{HBr}^+ + \text{CO}_2 \rightarrow \text{HOCO}^+ + \text{Br}^-$ Reaction^a

method	$\Delta_r E$	IM	v-IM	TS
aug-cc-pVDZ/PP	158	−656	−552	−463
aug-cc-pVTZ/PP	138	−736	−574	−482
aug-cc-pVQZ/PP	154	−780	−596	−484
CBS (aug-cc-pVXZ)/PP	166	−806	−610	−485
cc-pVDZ/PP	10	−670	−527	−442
cc-pVTZ/PP	38	−727	−535	−452
cc-pVQZ/PP	98	−706	−548	−448
CBS (cc-pVXZ)/PP	137	−690	−556	−445
experimental	50 ± 5	N/A	N/A	N/A

^aUnit of energies is meV.

reaction energy is 137 meV from cc-pVXZ/CBS and 166 meV from aug-cc-pVXZ/CBS. The levels of differences (87 and 116 meV) between experiments and CCSD(T) are close to the values previously reported for gas-phase reactions.^{51–53} It is worth pointing out that the reaction energy from our CCSD(T) calculation is slightly different from the numbers reported by Sun et al.¹⁶ The discrepancy comes from the different treatments of angular function. Cartesian angular functions (6d, 10f, 15g, ...) were used in Sun et al.,¹⁶ and in this study, we adapt spherical-harmonic (5d, 7f, 9g, ...) angular functions. We have experienced convergence issues in CCSD(T) calculations with Cartesian angular functions especially, when using quadruple basis sets.

Table 1 suggests that the nonaugmented basis sets (i.e., cc-pVXZ, X = D, T, Q) show consistently better agreement in reaction energy than the augmented basis sets (i.e., aug-cc-pVXZ, X = D, T, Q). Therefore, the energies from the CCSD(T)/CBS with the cc-pVXZ basis sets are considered to be more reliable in representing the potential energy profile of the reaction and are adapted as the benchmark energies in this study. There are two intermediates involved in the $\text{HBr}^+ + \text{CO}_2 \rightarrow \text{HOCO}^+ + \text{Br}^-$ reaction, and their geometries are

depicted in Figure 1. The hydrogen atom of HBr^+ could interact with either of the oxygen atoms in CO_2 to form a hydrogen bond complex, $[\text{BrH}-\text{OCO}]^+$, named IM in this Article. Alternatively, $\text{HBr}^+ + \text{CO}_2$ could form a van der Waals intermediate through an electrostatic interaction, named v-IM. Because the van der Waals interaction is generally weaker than the hydrogen bond interaction, the potential energy of the v-IM is ~ 130 meV higher than that of the IM according to the CCSD(T)/CBS/cc-pVXZ/PP calculation. The spin-free potential energies for the IM and v-IM from the CCSD(T)/cc-pVXZ/CBS up to the quadrupole- ζ basis set are -690 and -556 meV, respectively.

A transition state (TS) that connects the IM and v-IM is found (see Figure 2) and confirmed with IRC calculations for

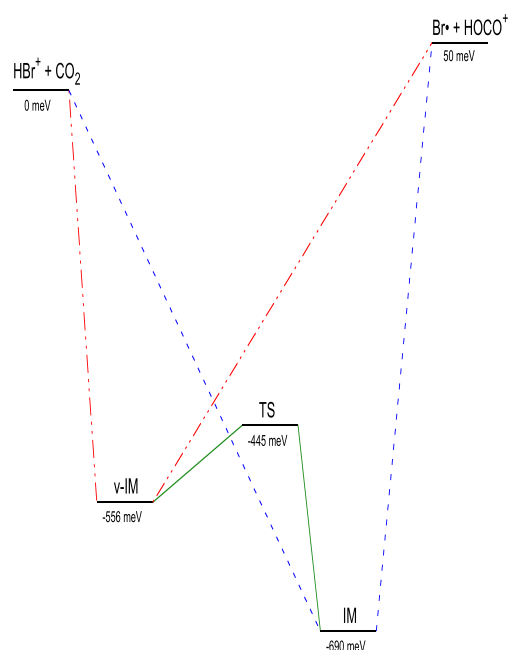


Figure 2. Benchmark potential energy profile of the $\text{HBr}^+ + \text{CO}_2 \rightarrow \text{HOCO}^+ + \text{Br}^-$ reaction. The energy values are calculated from CCSD/CBS/cc-pVXZ/pp, except for the reaction energy, which is from the experiment.^{7,8}

the $\text{HBr}^+ + \text{CO}_2 \rightarrow \text{HOCO}^+ + \text{Br}^-$ reaction, whose geometry is depicted in Figure 1. As shown in the structure of the TS, one oxygen atom of the CO_2 molecule is able to interact with both the hydrogen and the bromine of the HBr^+ molecule. The energy of the TS based on the CCSD(T)/cc-pVXZ/CBS calculation is -445 meV, which presents a potential energy barrier of 245 and 111 meV for IM and v-IM, respectively, to interconvert to one another. The IRC calculation also allows us to verify that no other reaction intermediates or transition states exist between the TS and IM or between the TS and v-IM. The benchmark potential energy profile of this reaction is depicted in Figure 1, and details of the CCSD(T) calculations are summarized in Table 1.

III.b. Potential Energy Profile from Single Reference Methods. As discussed in the Methods section, the benchmark for the reaction energy of the $\text{HBr}^+ + \text{CO}_2 \rightarrow \text{HOCO}^+ + \text{Br}^-$ reaction is chosen from the experimental value, 50 ± 5 meV. Table 2 lists all of the reaction energies calculated with varying single reference methods. The tested functionals include both more “traditional” ones, such as B3LYP and

Table 2. Summary of the Potential Energies (meV, without ZPE) Calculated from UMP2 and DFT Functionals with Various Basis Sets and ECP^a

basis set	method								
	B3LYP	B98	UMP2	M05	M06	XMVS15	M06-L	XM06	CM06-L
	Reaction Energy (Br + HOCO ⁺)								
aug-cc-pVDZ/LANL2DZdp	102	80	309	336	175	101	196	58	-262
aug-cc-pVDZ/PP	82	54	131	251	204	73	301	96	-275
aug-cc-pVDZ/LANL08	10	-25	356	223	57	-5	50	161	981
aug-cc-pVDZ/LANL08d	131	108	234	368	196	132	215	70	-286
cc-pVDZ/PP	-32	-38	-30	164	105	68	212	-174	-1365
cc-pVDZ/LANL08	-160	-159	34	92	-64	-46	-30	-265	-1179
cc-pVDZ/LANL08d	-11	3	-13	267	105	116	168	-336	-2381
cc-pVTZ/PP	50	23	65	147	141	-2	296	52	-636
benchmark energy					137 (50 ± 5)				
	IM								
aug-cc-pVDZ/LANL2DZdp	-731	-761	-660	-571	-644	-470	-637	-468	-1884
aug-cc-pVDZ/PP	-766	-801	-712	-651	-662	-516	-593	-445	-1652
aug-cc-pVDZ/LANL08	-776	-811	-605	-612	-703	-554	-689	-512	-1850
aug-cc-pVDZ/LANL08d	-713	-744	-646	-552	-633	-456	-629	-462	-1881
cc-pVDZ/PP	-869	-875	-739	-717	-731	-614	-653	-748	-2987
cc-pVDZ/LANL08	-851	-854	-503	-652	-732	-588	-695	-809	-2910
cc-pVDZ/LANL08d	-819	-819	-705	-617	-695	-576	-663	-799	-3446
cc-pVTZ/PP	-780	-816	-731	-704	-691	-565	-609	-522	-2227
benchmark energy					-690				
	v-IM								
aug-cc-pVDZ/LANL2DZdp	-705	-729	-515	-688	-609	-623	-864	-1113	-1877
aug-cc-pVDZ/PP	-727	-735	-550	-669	-683	-629	-823	-1071	-1917
aug-cc-pVDZ/LANL08	-707	-727	-498	-683	-759	-666	-894	N/A	-1850
aug-cc-pVDZ/LANL08d	-691	-716	-506	-676	-748	-612	-854	-1118	-1880
cc-pVDZ/PP	-845	-828	-515	-736	-752	-486	-882	-1370	-3148
cc-pVDZ/LANL08	-807	-802	-434	-735	-818	-556	-932	-1421	-3029
cc-pVDZ/LANL08d	-810	-808	-503	-755	-825	-524	-898	-1328	-3603
cc-pVTZ/PP	-731	-730	-532	-666	-686	-621	-793	-1224	-2465
benchmark energy					-556				
	TS								
aug-cc-pVDZ/LANL2DZdp	-503	-507	-460	-496	-516	-448	-778	N/A	-1723
aug-cc-pVDZ/PP	-519	-516	-486	-497	-484	-663	-744	N/A	N/A
aug-cc-pVDZ/LANL08	-520	-521	-467	-502	-533	-408	-674	N/A	N/A
aug-cc-pVDZ/LANL08d	-492	-498	-453	-487	-509	-436	-768	N/A	N/A
cc-pVDZ/PP	-619	-596	-451	-556	-542	-428	-673	N/A	N/A
cc-pVDZ/LANL08	-599	-582	-410	-541	-581	-801	-757	N/A	N/A
cc-pVDZ/LANL08d	-589	-573	-442	-534	-569	-628	-688	3421	N/A
cc-pVTZ/PP	-525	-518	N/A	-491	-487	-606	-560	N/A	N/A
benchmark energy					-445				

^aPotential energy of the reactants is set to zero. The benchmark energy is computed from CCSD(T)/CBS/cc-pVXZ, except for the reaction energy, which is from experiment.

B98, and more recently developed ones, such as M06 and XMVS15. UMP2 is also tested for its moderate computational cost.²⁸ The nonaugmented basis sets with UMP2 give the most accurate results in relation to the experimental value; in comparison, most of the reaction energies from the augmented basis sets are far too endothermic. Interestingly, a similar behavior is observed in the CCSD(T) calculation. (Please refer to Table 1.) For the DFT calculations, a general trend is not readily noticeable. For example, XMVS15 with all of the basis sets except aug-cc-pVDZ/LANL08d and cc-pVDZ/LANL08 gives a reaction energy within the range of roughly 70 meV of the benchmark. The XM06 functional with most of the augmented basis sets gives reaction energies within ~50 meV of the benchmark value, whereas most of the nonaugmented basis sets with this functional give largely negative reaction

energies. In addition, the CM06-L functional consistently gives an inaccurate reaction energy, especially with the non-augmented basis sets. The overall bad results of CM06-L are due to the inaccurate geometry of CO₂. Overall, almost every DFT functional gives at least a couple of good reaction energy values, but no definite trend can be found.

These two intermediates are likely to be populated by different orientations and impact parameters of the collision incident and clearly affect the reaction dynamics.^{13,35,36} Therefore, it is important to identify a good single reference method that reproduces the potential energy of the v-IM and the IM for the AIMD simulations. The performance of UMP2 and DFTs on the v-IM and IM varies, and the trend is somewhat unclear. Some of the functionals predict the v-IM to hold a similar or lower potential energy than the IM (e.g., most

Table 3. rmsd Values (meV) of Each Single Reference Method Compared with the Benchmark PES^a

basis set	method								
	B3LYP	B98	UMP2	M05	M06	XMVS15	M06-L	XM06	CM06-L
aug-cc-pVDZ/LANL2DZdp	87	99	132	170	80	118	240	N/A	1107
aug-cc-pVDZ/PP	102	111	47	120	103	145	241	N/A	N/A
aug-cc-pVDZ/LANL08	97	118	162	118	111	93	204	N/A	N/A
aug-cc-pVDZ/LANL08d	83	93	98	184	128	127	237	N/A	N/A
cc-pVDZ/PP	195	186	51	121	115	53	216	N/A	N/A
cc-pVDZ/LANL08	198	193	114	105	160	192	247	N/A	N/A
cc-pVDZ/LANL08d	163	157	42	158	151	114	218	1981	N/A
cc-pVTZ/PP	106	114	N/A	77	82	110	185	N/A	N/A

^a“N/A” indicates that at least one of IM, v-IM, or TS was not found with the respective method.

of M05 except for cc-pVTZ/PP; and some results from different versions of M06), possibly due to an overestimation of the van der Waals interaction. In the hope of better characterizing the long-range interaction in v-IM and IM, DFTs with various dispersion corrections^{54,55} are tested, but the results are not consistent and do not improve the overall performance (results not shown). In addition, some of the dispersion corrections were not available for all of the functionals that are tested in this study. Even though there are mixed results for most of the functionals and basis sets, interestingly, CM06-L with all basis sets again gives consistently inaccurate values. MP2 shows an overall superior performance to DFTs, especially with aug-cc-pVDZ/PP and cc-pVDZ/LANL08d. The only DFT method that predicts a reasonable energy of v-IM is XMVS15 with cc-pVDZ/LANL08, cc-pVDZ/LANL08d, and cc-pVDZ/PP.

III.c. Identifying the Optimal Method for the AIMD Simulation. The rmsd values of the four points on the PES (e.g., reaction energy, IM, v-IM, and TS) from each single reference method are calculated and summarized in Table 3. The candidate methods are evaluated according to three criteria: (1) a relatively low rmsd value (~ 50 meV), (2) an accurate representation of the reaction energy (close to 50 meV), and (3) a reliable representation of the relative energies between the critical points (IM, v-IM, and TS).

The first criteria eliminate most of the combinations of methods and basis sets for the AIMD simulations. It is worth noting that almost all of the DFT functionals with the triple- ζ basis set (e.g., cc-pVTZ/PP) give a relatively low rmsd value. However, as previously stated, a triple- ζ basis set requires much more time for each energy gradient calculation than a double- ζ basis set and therefore will not be considered as an optimal method for the AIMD simulations. The four smallest rmsd values, from the lowest to the highest, are UMP2/cc-pVDZ/LANL08d, UMP2/aug-cc-pVDZ/PP, UMP2/cc-pVDZ/PP, and XMVS15/cc-pVDZ/PP. Among the three UMP2 calculations, the aug-cc-pVDZ/PP has the largest number of basis functions, and its performance does not give the lowest rmsd, so it will not be considered any further. The difference between the rmsd values of UMP2/cc-pVDZ/lanl08d and UMP2/cc-pVDZ/PP is only 9 meV. The UMP2/cc-pVDZ/lanl08d is chosen as the optimal MP2 method for the following three reasons:

- (a) Better relative energy between the three intermediates: The relative energy differences between TS and IM, TS and v-IM, and v-IM and IM from the benchmark are 245, 111, and 134 meV, respectively. Overall, UMP2/cc-pVDZ/lanl08d outperforms other candidate methods in

representing the intermediates and the transition state of this reaction.

- (b) Better representation of the reaction energy: -30 meV from the UMP2/cc-pVDZ/PP compared with -13 meV from the UMP2/cc-pVDZ/lanl08d (benchmark value is 50 meV).
- (c) Smaller basis set: There are 71 basis functions in the UMP2/cc-pVDZ/lanl08d, which is four fewer basis functions than the UMP2/cc-pVDZ/PP calculation.

The DFT method with the lowest rmsd (53 meV) is XMVS15/cc-pVDZ/PP. The reaction energy is accurately represented (68 meV), and the energy of the intermediates agrees reasonably well with the benchmark. We decided to report XMVS15/cc-pVDZ/PP as a backup candidate method for AIMD simulations because its rmsd is slightly higher than that of UMP2/cc-pVDZ/lanl08d. The preference of the UMP2/cc-pVDZ/lanl08d method for the AIMD study is due to our previous experiences with guided ion beam simulations. Similar to the reaction of $\text{HBr}^+ + \text{CO}_2 \rightarrow \text{HOCO}^+ + \text{Br}$, the PES of the reaction of $\text{F}^- + \text{CH}_3\text{I} \rightarrow \text{CH}_3\text{F} + \text{I}^-$ could be represented by one DFT method (B3LYP/6-31G*) and one MP2 method (MP2/cc-pVDZ) with almost equal accuracy.^{13,35,56} However, the dynamics of the reaction from simulations with these theories were vastly different: The reaction cross section predicted from the AIMD MP2 simulations ($1.8 \pm 0.3 \text{ \AA}^2$) was less than a quarter of the reaction cross section predicted from the AIMD DFT simulations ($8.6 \pm 2.2 \text{ \AA}^2$), and the scattering angle distribution from the MP2 AIMD simulations showed a much better agreement with the experiment than the B3LYP AIMD simulations. Interestingly, similar to this reaction, the DFT method also showed better reaction energy than the MP2 method in the reaction of $\text{F}^- + \text{CH}_3\text{I} \rightarrow \text{CH}_3\text{F} + \text{I}^-$. This is probably due to the fact that DFTs focus on reproducing the energy of the optimal structures, which could potentially lead to an underfitting for the unoptimized structures that are very common in a dynamic simulation.

IV. DISCUSSION

The goal of this study is to characterize the potential energy profile of $\text{HBr}^+ + \text{CO}_2 \rightarrow \text{HOCO}^+ + \text{Br}$ and search for a better cost-effective combination of a single reference method (DFT or MP2) and a basis set with an ECP for our future AIMD simulations. This reaction showed very interesting responses to various excitations (refer to the Introduction), indicating a complicated potential energy landscape that populates different reaction pathways. Two intermediates (one hydrogen bond complex, IM, and one van der Waals complex, v-IM) had been

previously reported, but how they are related to each other remained unknown. Therefore, a transition-state search was performed, and a transition state (i.e., TS in Figures 1 and 2) that connects IM and v-IM was indeed found. The TS was further verified with frequency and IRC calculations, which also showed that no other transition state exists between the IM and the v-IM.

With the discovery of the TS, the reaction PES became double-welled and was composed of a prereaction complex, a postreaction complex, and a transition state connecting them. A double-welled PES has been reported to show great complexity in populating different reaction pathways under different collision energies and impact parameters.^{56–60} For example, the PES of the nucleophilic substitution reaction, $F^- + CH_3Cl \rightarrow CH_3F + Cl^-$, contains one prereaction complex ($[F-CH_3Cl]^-$, C_{3v} symmetry), one transition state ($[F-CH_3-Cl]^-$, C_{3v} symmetry), and one postreaction complex ($[FCH_3-Cl]^-$, C_{3v} symmetry). Three different pathways have been found for this reaction:

- Direct rebound: F^- collides almost colinearly (along the C–Cl axis) with C and immediately repels Cl^- . This is the “traditional” mechanism of a nucleophilic substitution reaction.
- Direct strip: F^- collides almost vertically (to the C–Cl axis) with C and immediately repels Cl^- .
- Indirect: F^- collides with CH_3Cl and forms an intermediate complex that has a measurable lifetime before it eventually dissociates to products (CH_3F and Cl^-).

At a low collision energy, pathway (c) is the most populated, and the reaction shows isotropic scattering; at high collision energy, pathway (a) is the most popular, and the reaction shows forward scattering. Similarly, we expect that various excitations will populate different reaction pathways in the $HBr^+ + CO_2 \rightarrow HOCO^+ + Br\cdot$ reaction, which might lead to different reaction cross sections, energy distributions of the products, and scattering angles of the products. What makes this reaction even more interesting is that unlike the nucleophilic substitution, where the pre- and postreaction complexes are well-defined, either the IM or the v-IM in the $HBr^+ + CO_2 \rightarrow HOCO^+ + Br\cdot$ reaction can be the pre- or the postreaction complex, depending on the orientation of the collision. This is supported by preliminary results from AIMD (with UMP2/cc-pVDZ/lanl08d energy gradient), which show that both IM and v-IM could form after the collision. (See Figures S1 and S2.) The reaction dynamics of the gas phase assumes that intermediates (IM and v-IM) can interconvert to each other through transition states and intermediates can dissociate to products ($HOCO^+ + Br\cdot$).¹ As a result, the dynamics of this reaction is expected to be much more complicated, and indirect mechanics could play a predominant role.

In summary, we have tested various combinations of single reference methods (DFTs and MP2) and basis sets to search for the most cost-effective method for the AIMD simulation study of the $HBr^+ + CO_2 \rightarrow HOCO^+ + Br\cdot$ reaction. UMP2/cc-pVDZ/lanl08d and XMVS15/cc-pVDZ/PP have been chosen for their accurate representation of reaction energy and relative energies of the IM, TS, and v-IM. These methods significantly reduce the computation cost up to 90% in comparison with the previously suggested UMP2/cc-pVTZ/PP method.¹⁶ With the knowledge of the potential energy

profile and an appropriate ab initio method, the simulation of the $HBr^+ + CO_2 \rightarrow HOCO^+ + Br\cdot$ reaction is currently running to reveal the nature between the excitation and the reaction dynamics of the specific ion–molecule reaction. To the best of our knowledge, atomistic reaction dynamics has not been previously studied for an ion–molecule reaction with a double-welled potential, where the pre- and the postreaction complexes could not be readily defined. The dynamics of this reaction is currently being simulated.

■ ASSOCIATED CONTENT

📄 Supporting Information

The Supporting Information is available free of charge on the ACS Publications website at DOI: 10.1021/acs.jpca.9b07651.

Table S1. Vibrational modes of intermediates and transition states of the $HBr^+ + CO_2 \rightarrow HOCO^+ + Br\cdot$ reaction. Figures S1 and S2. Snapshots of AIMD (PDF)

■ AUTHOR INFORMATION

Corresponding Author

*E-mail: ruisun@hawaii.edu.

ORCID

Jiaxu Zhang: 0000-0002-3125-7824

Li Yang: 0000-0002-0143-3524

Rui Sun: 0000-0003-0638-1353

Notes

The authors declare no competing financial interest.

■ ACKNOWLEDGMENTS

We thank Dr. Theresa Windus from Iowa State University for fruitful discussions. We thank the information technology service (ITS) from the University of Hawai'i, Manoa and XSEDE⁶¹ for the computational resources. We are grateful for the financial support from the University of Hawai'i, Manoa.

■ REFERENCES

- Steinfeld, J. I.; Francisco, J. S.; Hase, W. L. *Chemical Kinetics and Dynamics*; Prentice Hall, 1999.
- Truhlar, D. G.; Hase, W. L.; Hynes, J. T. Current Status of Transition-State Theory. *J. Phys. Chem.* **1983**, *87* (15), 2664–2682.
- Di Giacomo, F. A Short Account of RRKM Theory of Unimolecular Reactions and of Marcus Theory of Electron Transfer in a Historical Perspective. *J. Chem. Educ.* **2015**, *92* (3), 476–481.
- Langer, W. D.; Graedel, T. E. Ion–Molecule Chemistry of Dense Interstellar Clouds–Nitrogen-, Oxygen-, and Carbon-Bearing Molecule Abundances and Isotopic Ratios. *Astrophys. J., Suppl. Ser.* **1989**, *69*, 241–269.
- Williams, K. L.; Martin, I. T.; Fisher, E. R. On the Importance of Ions and Ion–Molecule Reactions to Plasma–Surface Interface Reactions. *J. Am. Soc. Mass Spectrom.* **2002**, *13* (5), 518–529.
- Osburn, S.; Ryzhov, V. Ion–Molecule Reactions: Analytical and Structural Tool. *Anal. Chem.* **2013**, *85* (2), 769–778.
- Paetow, L.; Unger, F.; Beichel, W.; Frenking, G.; Weitzel, K. M. Rotational Dependence of the Proton-Transfer Reaction $HBr^+ + CO_2 \rightarrow HOCO^+ + Br\cdot$. I. Energy versus Angular Momentum Effects. *J. Chem. Phys.* **2010**, *132* (17), 174305.
- Paetow, L.; Unger, F.; Beutel, B.; Weitzel, K.-M. Rotational Dependence of the Proton-Transfer Reaction $HBr^+ + CO_2 \rightarrow HOCO^+ + Br\cdot$. II. Comparison of $HBr^+ (^2\Pi_{3/2})$ and $HBr^+ (^2\Pi_{1/2})$. *J. Chem. Phys.* **2010**, *133* (23), 234301.
- Payne, M.; Teter, M.; Allan, D.; Arias, T.; Joannopoulos, J. Iterative Minimisation Techniques for Ab Initio Total Energy Calculations MD and CG. *Rev. Mod. Phys.* **1992**, *64* (4), 1045–1097.

- (10) Pratihari, S.; Ma, X.; Homayoon, Z.; Barnes, G. L.; Hase, W. L. Direct Chemical Dynamics Simulations. *J. Am. Chem. Soc.* **2017**, *139* (10), 3570–3590.
- (11) Tuckerman, M. E. Ab Initio Molecular Dynamics: Basic Concepts, Current Trends and Novel Applications. *J. Phys.: Condens. Matter* **2002**, *14* (50), R1297–R1355.
- (12) Lourderaj, U.; Park, K.; Hase, W. L. Classical Trajectory Simulations of Post-Transition State Dynamics. *Int. Rev. Phys. Chem.* **2008**, *27*, 361–403.
- (13) Sun, R.; Davda, C. J.; Zhang, J.; Hase, W. L. Comparison of Direct Dynamics Simulations with Different Electronic Structure Methods. $F^- + CH_3I$ with MP2 and DFT/B97–1. *Phys. Chem. Chem. Phys.* **2015**, *17* (4), 2589–2597.
- (14) Gross, E. K. U.; Dreizler, R. M. *Density Functional Theory*; Springer Science & Business Media, 2013.
- (15) Møller, C.; Plesset, M. S. Note on an Approximation Treatment for Many-Electron Systems. *Phys. Rev.* **1934**, *46* (7), 618–622.
- (16) Sun, R.; Granucci, G.; Paul, A. K.; Siebert, M.; Liang, H. J.; Cheong, G.; Hase, W. L.; Persico, M. Potential Energy Surfaces for the $HBr^+ + CO_2 \rightarrow Br + HOCO^+$ Reaction in the $HBr^+ \ ^2\Pi_{3/2}$ and $^2\Pi_{1/2}$ Spin-Orbit States. *J. Chem. Phys.* **2015**, *142* (10), 104302.
- (17) Raghavachari, K.; Trucks, G. W.; Pople, J. A.; Head-Gordon, M. A Fifth-order Perturbation Comparison of Electron Correlation Theories. *Chem. Phys. Lett.* **1989**, *157* (6), 479–483.
- (18) Szabo, A.; Ostlund, N. S. *Modern Quantum Chemistry: Introduction to Advanced Electronic Structure Theory*; Dover Publications: New York, 1996.
- (19) Peterson, K. A.; Woon, D. E.; Dunning, T. H. Benchmark Calculations with Correlated Molecular Wave Functions. IV. The Classical Barrier Height of the $H + H_2 \rightarrow H_2 + H$ Reaction. *J. Chem. Phys.* **1994**, *100* (10), 7410–7415.
- (20) Varandas, A. J. C. Basis-Set Extrapolation of the Correlation Energy. *J. Chem. Phys.* **2000**, *113* (20), 8880–8887.
- (21) Ross, R. B.; Gayen, S.; Ermler, W. C. Ab Initio Relativistic Effective Potentials with Spin-Orbit Operators. V. Ce through Lu. *J. Chem. Phys.* **1994**, *100* (11), 8145–8155.
- (22) Krauss, M.; Stevens, W. J. Effective Potentials in Molecular Quantum Chemistry. *Annu. Rev. Phys. Chem.* **1984**, *35*, 357–385.
- (23) Dolg, M.; Cao, X. Relativistic Pseudopotentials: Their Development and Scope of Applications. *Chem. Rev.* **2012**, *112* (1), 403–480.
- (24) Valiev, M.; Bylaska, E. J.; Govind, N.; Kowalski, K.; Straatsma, T. P.; Van Dam, H. J. J.; Wang, D.; Nieplocha, J.; Apra, E.; Windus, T. L.; et al. NWChem: A Comprehensive and Scalable Open-Source Solution for Large Scale Molecular Simulations. *Comput. Phys. Commun.* **2010**, *181* (9), 1477–1489.
- (25) Zhao, Y.; Schultz, N. E.; Truhlar, D. G. Design of Density Functionals by Combining the Method of Constraint Satisfaction with Parameterization for Thermochemistry, Thermochemical Kinetics, and Noncovalent Interactions. *J. Chem. Theory Comput.* **2006**, *2* (2), 364–382.
- (26) Zhao, Y.; Truhlar, D. G. A New Local Density Functional for Main-Group Thermochemistry, Transition Metal Bonding, Thermochemical Kinetics, and Noncovalent Interactions. *J. Chem. Phys.* **2006**, *125* (19), 194101.
- (27) Zhao, Y.; Truhlar, D. G. Hybrid Meta Density Functional Theory Methods for Thermochemistry, Thermochemical Kinetics, and Noncovalent Interactions: The MPW1B95 and MPWB1K Models and Comparative Assessments for Hydrogen Bonding and van Der Waals Interactions. *J. Phys. Chem. A* **2004**, *108* (33), 6908–6918.
- (28) Zheng, J.; Zhao, Y.; Truhlar, D. G. Representative Benchmark Suites for Barrier Heights of Diverse Reaction Types and Assessment of Electronic Structure Methods for Thermochemical Kinetics. *J. Chem. Theory Comput.* **2007**, *3* (2), 569–582.
- (29) Becke, A. D. Density-Functional Thermochemistry. IV. A New Dynamical Correlation Functional and Implications for Exact-Exchange Mixing. *J. Chem. Phys.* **1996**, *104* (3), 1040–1046.
- (30) Schmider, H. L.; Becke, A. D. Optimized Density Functionals from the Extended G2 Test Set. *J. Chem. Phys.* **1998**, *108* (23), 9624–9631.
- (31) Sun, J.; Perdew, J. P.; Ruzsinszky, A. Semilocal Density Functional Obeying a Strongly Tightened Bound for Exchange. *Proc. Natl. Acad. Sci. U. S. A.* **2015**, *112* (3), 685–689.
- (32) Dunning, T. H. Gaussian Basis Sets for Use in Correlated Molecular Calculations. I. The Atoms Boron through Neon and Hydrogen. *J. Chem. Phys.* **1989**, *90* (2), 1007–1023.
- (33) Wilson, A. K.; Woon, D. E.; Peterson, K. A.; Dunning, T. H. Gaussian Basis Sets for Use in Correlated Molecular Calculations. IX. The Atoms Gallium through Krypton. *J. Chem. Phys.* **1999**, *110* (16), 7667–7676.
- (34) Peterson, K. A.; Figgen, D.; Goll, E.; Stoll, H.; Dolg, M. Systematically Convergent Basis Sets with Relativistic Pseudopotentials. II. Small-Core Pseudopotentials and Correlation Consistent Basis Sets for the Post-d Group 16 – 18 Elements Systematically Convergent Basis Sets with Relativistic Pseudopotentials. *J. Chem. Phys.* **2003**, *119*, 11113.
- (35) Mikosch, J.; Zhang, J.; Trippel, S.; Eichhorn, C.; Otto, R.; Sun, R.; De Jong, W. A.; Weidemüller, M.; Hase, W. L.; Wester, R. Indirect Dynamics in a Highly Exoergic Substitution Reaction. *J. Am. Chem. Soc.* **2013**, *135* (11), 4250–4259.
- (36) Zhang, J.; Lourderaj, U.; Sun, R.; Mikosch, J.; Wester, R.; Hase, W. L. Simulation Studies of the $Cl^- + CH_3I$ S_N2 Nucleophilic Substitution Reaction: Comparison with Ion Imaging Experiments. *J. Chem. Phys.* **2013**, *138* (11), 114309.
- (37) Ruscic, B.; Pinzon, R. E.; Morton, M. L.; von Laszewski, G.; Bittner, S. J.; Nijssure, S. G.; Amin, K. A.; Minkoff, M.; Wagner, A. F. Introduction to Active Thermochemical Tables: Several “Key” Enthalpies of Formation Revisited. *J. Phys. Chem. A* **2004**, *108* (45), 9979–9997.
- (38) Wilson, E. B.; Decius, J. C.; Cross, P. C. *Molecular Vibrations: The Theory of Infrared and Raman Vibrational Spectra*; Dover Books on Chemistry Series; Dover Publications, 1980.
- (39) Levine, I. N. *Molecular Spectroscopy*; Wiley-Interscience, 1975.
- (40) Petty, J. T.; Moore, C. B. Transient Infrared Absorption Spectrum of the N1 Fundamental of Trans-HOCO. *J. Mol. Spectrosc.* **1993**, *161* (1), 149–156.
- (41) Sears, T. J.; Fawzy, W. M.; Johnson, P. M. Transient Diode Laser Absorption Spectroscopy of the ν_2 Fundamental of Trans-HOCO and DOCO. *J. Chem. Phys.* **1992**, *97* (6), 3996–4007.
- (42) Johnson, C. J.; Harding, M. E.; Poad, B. L. J.; Stanton, J. F.; Continetti, R. E. Electron Affinities, Well Depths, and Vibrational Spectroscopy of Cis - And Trans -HOCO. *J. Am. Chem. Soc.* **2011**, *133* (49), 19606–19609.
- (43) Forney, D.; Jacox, M. E.; Thompson, W. E. Infrared Spectra of Trans-HOCO, $HCOOH^+$, and HCO_2 -Trapped in Solid Neon. *J. Chem. Phys.* **2003**, *119* (20), 10814–10823.
- (44) Tech, J. L. Analysis of the Spectrum of Neutral Atomic Bromine (Br I). *J. Res. Natl. Bur. Stand., Sect. A* **1963**, *67A* (6), 505.
- (45) Harvey, J. S. M.; Kamper, R. A.; Lea, K. R. Paramagnetic Resonance Absorption in Bromine and Chlorine. *Proc. Phys. Soc., London* **1960**, *76* (6), 979.
- (46) Davies, P. B.; Thrush, B.; Stone, A.; Wayne, F. The Gas-Phase Electron Paramagnetic Resonance Spectrum of Excited ($4p^5 3p^2$) Bromine Atoms. *Chem. Phys. Lett.* **1972**, *17* (1), 19–21.
- (47) Peterson, K. A. Systematically Convergent Basis Sets with Relativistic Pseudopotentials. I. Correlation Consistent Basis Sets for the Post-d Group 13–15 Elements. *J. Chem. Phys.* **2003**, *119* (21), 11099–11112.
- (48) Fukui, K. Formulation of the Reaction Coordinate. *J. Phys. Chem.* **1970**, *74* (23), 4161–4163.
- (49) Maeda, S.; Harabuchi, Y.; Ono, Y.; Taketsugu, T.; Morokuma, K. Intrinsic Reaction Coordinate: Calculation, Bifurcation, and Automated Search. *Int. J. Quantum Chem.* **2015**, *115* (5), 258–269.
- (50) Ischtwan, J.; Collins, M. A. Determination of the Intrinsic Reaction Coordinate: Comparison of Gradient and Local Quadratic Approximation Methods. *J. Chem. Phys.* **1988**, *89* (5), 2881–2885.

(51) Sun, R.; Xie, J.; Zhang, J.; Hase, W. L. The $F^- + CH_3I \rightarrow FCH_3 + I^-$ Entrance Channel Potential Energy Surface Comparison of Electronic Structure Methods. *Int. J. Mass Spectrom.* **2015**, *377* (1), 222–227.

(52) Zhang, J.; Lourderaj, U.; Addepalli, S. V.; de Jong, W. A.; Hase, W. L. Quantum Chemical Calculations of the $Cl^- + CH_3I \rightarrow CH_3Cl + I^-$ Potential Energy Surface. *J. Phys. Chem. A* **2009**, *113* (10), 1976–1984.

(53) Zhang, J.; Hase, W. L. Electronic Structure Theory Study of the $F^- + CH_3I \rightarrow FCH_3 + I^-$ Potential Energy Surface. *J. Phys. Chem. A* **2010**, *114* (36), 9635–9643.

(54) Wu, Q.; Yang, W. Empirical Correction to Density Functional Theory for van Der Waals Interactions. *J. Chem. Phys.* **2002**, *116* (2), 515–524.

(55) Zimmerli, U.; Parrinello, M.; Koumoutsakos, P. Dispersion Corrections to Density Functionals for Water Aromatic Interactions. *J. Chem. Phys.* **2004**, *120* (6), 2693–2699.

(56) Sun, R.; Xie, J.; Zhang, J.; Hase, W. L. The $F^- + CH_3I \rightarrow FCH_3 + I^-$ Entrance Channel Potential Energy Surface Comparison of Electronic Structure Methods. *Int. J. Mass Spectrom.* **2015**, *377* (1), 222–227.

(57) Su, T.; Wang, H.; Hase, W. L. Trajectory Studies of SN_2 Nucleophilic Substitution. 7. $F^- + CH_3Cl \rightarrow FCH_3 + Cl^-$. *J. Phys. Chem. A* **1998**, *102*, 9819–9828.

(58) Wang, H.; Hase, W. L. Kinetics of $F^- + CH_3Cl$ SN_2 Nucleophilic Substitution. *J. Am. Chem. Soc.* **1997**, *119* (13), 3093–3102.

(59) Yang, L.; Zhang, J.; Xie, J.; Ma, X.; Zhang, L.; Zhao, C.; Hase, W. L. Competing E_2 and SN_2 Mechanisms for the $F^- + CH_3CH_2I$ Reaction. *J. Phys. Chem. A* **2017**, *121* (5), 1078–1085.

(60) Zhang, J.; Yang, L.; Xie, J.; Hase, W. L. Microsolvated $F^-(H_2O) + CH_3I$ SN_2 Reaction Dynamics. Insight into the Suppressed Formation of Solvated Products. *J. Phys. Chem. Lett.* **2016**, *7* (4), 660–665.

(61) Towns, J.; Cockerill, T.; Dahan, M.; Foster, I.; Gaither, K.; Grimshaw, A.; Hazlewood, V.; Lathrop, S.; Lifka, D.; Peterson, G. D.; et al. XSEDE: Accelerating Scientific Discovery. *Comput. Sci. Eng.* **2014**, *16* (5), 62–74.